Mitigating Metal Dendrite Formation in Lithium−Sulfur Batteries via Morphology-Tunable Graphene Oxide Interfaces

Yu-Ting Chen,[†] Syed Ali Abbas,[‡,†] Nahid Kaisar,[#,†] Sheng Hui Wu,[∥] Hsin-An Chen,[†] Karunakara Moorthy Boopathi,[†] Mriganka Singh,[†,§] Jason Fang,[∥] Chun-Wei Pao,[†] and Chih-Wei Chu*,[†,¶,∇]

[†]Research Center of Applied Sciences, Academia Sinica, Taipei 115, Taiwan

[¶]College of Engineering, Chang Gung University, Guishan District, Taoyuan City 33302, Taiwan

[∇]Department of Materials Science and Engineering and [‡]Department of Engineering and Systems Science, National Tsing Hua University, Hsinchu 30013, Taiwan

[§]Department of Materials Science and Engineering, National Chiao Tung University, Hsinchu 30010, Taiwan

[∥]Material and Chemical Research Laboratories, Industrial Technology Research Institute, Hsinchu 31040, Taiwan

[#]Department of Materials Science and Engineering, National Taiwan University of Science and Technology, Taipei 106, Taiwan

S *Supporting Information*

ABSTRACT: Despite issues related to dendrite formation, research on Li metal anodes has resurged because of their high energy density. In this study, graphene oxide (GO) layers are decorated onto Li metal anodes through a simple process of drop-casting and spray-coating. The self-assembly of GO is exploited to synthesize coatings having compact, mesoporous, and macroporous morphologies. The abilities of the GO coatings to suppress dendrite formation are compared through Li|Li symmetrical cell charging at a current density of 5 mA cm^{-2} for 2000 cycles—a particularly abusive test. The macroporous structure possesses the lowest impedance, whereas the compact structure excels in terms of stability. Moreover, GO exhibits a low nucleation overpotential and is transformed into reduced GO with enhanced conductivity during the operation of the cells; both factors synergistically mitigate the issue of dendrite formation. Li−S batteries incorporating the GO-decorated Li anodes exhibit an initial capacity of 850 mA h g^{-1} and maintain their stability for 800 cycles at a C-rate of 1 C (1675 mA h g^{-1}), suggesting the applicability of GO in future rechargeable batteries.

KEYWORDS: graphene oxide, lithium dendrites, lithium metal anodes, lithium−sulfur batteries, Li−S batteries
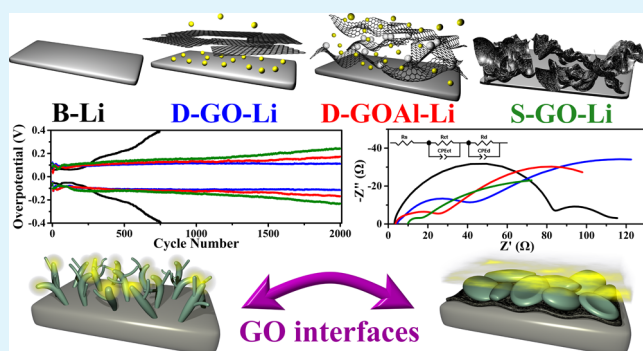
■ INTRODUCTION

Lithium anodes have been hailed as one of the most propitious energy storage media for fulfilling the requirements of proliferating electronic gadgets and vehicles, thanks to an unmatched high theoretical capacity (3860 mA h g^{-1}) and low redox potential (-3.04 V vs H$_2$/H$^+$).[1−3] Nevertheless, dendrite formation on Li anodes during cycling remains a lingering problem: not only does it increase the impedance of the cell, but also it poses a severe safety threat.[4−7] Therefore, LiX compounds (X = Al, Si, and, especially, C) of lower capacity are currently employed in commercial batteries, even though Li anodes were demonstrated earlier than any of those LiX materials.[8] Because it is more difficult to suppress dendrite formation during cycling, owing to the low surface energy and high migration energy of Li relative to other metals (e.g., Mg),[9,10] extra effort will have to be invested to tackle this issue.

Plating Li unevenly results in a lower effective reaction area and causes localization of the current density, thereby promoting Li dendrite formation.[11] Hence, controlling the incipient nucleation sites should significantly impact the subsequent Li plating process. Various factors influence the nucleation process: for example, the number density and the reciprocal of the average size of the nuclei are both proportional to the current density.[12] Furthermore, low or no nucleation potentials were observed when lithiophilic substrates or nuclei were employed, due to the formation of a solid solution buffer layer prior to plating the Li metal.[13,14] Other than regulating the nucleation process, several strategies have been proposed to suppress the formation of Li dendrites.

Placing a material of high dielectric constant (e.g., glass fibers)[15] or adding Cs^+ ions into the electrolytes[16] can dissipate the concentrated electronic field near the dendrite tips and, thus, hamper the aggressive growth of Li dendrites. Composite anodes fabricated using direct electrodeposition or molten Li reactions possess high capacities and a good ability to suppress dendrites.[4,17] Solid-state electrolytes of high modulus have proven effective at stopping the formation of Li dendrites[18] and have also been applied to full cells.[19] Nevertheless, the use of precious materials, the need for intricate techniques, and the inclusion of excessive non-active materials can all compromise the suitability of such approaches in commercial applications.

Carbon is one of the most promising materials for coating Li anodes for scalable production, because of its light weight, high abundance, mechanical and chemical stability, and ability to transport Li ions. Although several reports have described the lower propensity for Li dendrite formation in graphite microtube-, graphene oxide (GO)-, and carbon nanotube-modified Li anodes,[4,5,17,20−23] these approaches remain flawed. None of them satisfies the following three criteria simultaneously: (i) fabrication through simple techniques that are potentially commercializable; (ii) incorporation of low amounts of non-active materials; and (iii) a well-established relationship among the coating procedure, the surface morphologies, and the cycling performance. Moreover, most of the associated durability tests have been conducted at a current density of less than 5 mA cm^{-2} and have been limited to within 1000 cycles—conditions that will not satisfy the requirements for next-generation Li batteries.

On one hand, Li−S systems are among the most attractive for next-generation battery usage, because of a high theoretical capacity (1675 mA h g^{-1}), low cost, and environmental benignancy.[24,25] When combined with Li anodes, the energy density can reach as high as 2600 W h kg^{-1}.[25] Nevertheless, diffusion of soluble polysulfide intermediates during cell operation, the so-called "shuttle effect", and Li dendrite formation have both hampered the commercialization of Li−S batteries.[26−28] Although most research on Li−S batteries has focused on tackling the shuttle effect, prevention of Li dendrites remains an important issue that cannot be ignored.[20]

In this study, GO films were coated onto Li anodes using spray-coating and drop-casting methods—both suitable for commercial application—to suppress the formation of Li dendrites. By varying the coating conditions, the GO self-assembled into three different morphologies: compact, mesoporous, and macroporous structures. The modified Li anodes all passed a 2000 cycle test at a current density of 5 mA cm^{-2}—as such, they have among the longest life spans reported to date. The electrochemical performance differed depending upon the morphology of the GO coating: the macroporous structure possessed the lowest degrees of charge transfer and diffusion impedance, while the compact structure outperformed in terms of durability. During cycling, the GO coating transformed into reduced GO and could serve as both a conductive[29] and lithiophilic[17] substrate that synergistically suppressed the formation of Li dendrites. Furthermore, these coatings could be coupled with Li−S cells. The cells exhibited a capacity of 850 mA h g^{-1} after the first discharge and maintained a capacity of 400 mA h g^{-1} after 800 cycles at a C-rate of 1 C (1 C = 1675 mA h g^{-1})—this performance was 30% better than that of the noncoated counterpart.

■ EXPERIMENTAL SECTION

GO-Coated Li Foil. GO dry powder was obtained by vacuum-drying a GO aqueous slurry (Conjutek, Taiwan) at room temperature for 3 days. A GO solution at a concentration of 2 g L^{-1} was prepared by dispersing GO powder into tetrahydrofuran (THF) through sonication for 3 h. THF was chosen because of its good ability to disperse GO,[30,31] its low boiling point (to accelerate the evaporation process), and its high chemical stability against Li metal. A GO−Al_2O_3 solution at a concentration of 2 g L^{-1} GO and 1 g L^{-1} Al_2O_3 was prepared by mixing GO and Al_2O_3 nanoparticles (Sigma-Aldrich; particle size ≥ 50 nm) at a weight ratio of 2:1 and dispersing in THF through sonication for 3 h. The solutions were coated onto bare Li foil (B-Li) heated to 40 °C on a hot plate through drop-casting and spray-coating inside an Ar-filled glove box. Three modified samples were prepared: two from the GO solutions coated onto the Li foil through drop-casting (D-GO-Li; 0.2 mg cm^{-2} GO; see Figure S1, Supporting Information) and spray-coating (S-GO-Li; the spray gun was held at an altitude of 10 cm; spraying was stopped after a uniform black surface had formed) and one from the GO−Al_2O_3 solution through drop-casting (D-GOAl-Li; 0.2 mg cm^{-2} GO and 0.1 mg cm^{-2} Al_2O_3).

Expanded Graphite−Sulfur (EG:S) Cathode. Non-expanded graphite powder (Homytech, Taiwan) was transformed into EG flakes by heating at 800 °C for 1 h; the acquired EG flakes were impregnated with sulfur by heating an EG/S mixture at a weight ratio of 1:4 at 160 °C for 6 h in an autoclave to obtain the EG:S cathode material. A cathode slurry was prepared by ball-milling EG:S, super P, and poly(vinylidene fluoride) (PVDF) at a weight ratio of 7:2:1 with a suitable amount of N-methylpyrrole (NMP) for 4 h. The cathode was acquired by coating the slurry onto a piece of Al foil with a 300 μm doctor blade and then drying at 50 °C for 24 h. The sulfur loading was 2 mg cm^{-1}.

Electrochemical Measurements. All electrochemical measurements were conducted with a Celgard 2500 separator and electrodes encapsulated in CR2032 coin cells inside an Ar-filled glove box. In the Li|Li symmetrical tests, two pieces of round Li foil having a diameter of 14 mm were placed on both sides of the separator, with the coating facing the separator, if there was any. The electrolyte was 1 M bis(trifluoromethane)sulfonamide (LiTFSI) in dioxolane (DOL) and dimethoxyethane (DME) (1:1, v/v). The symmetrical cells were tested using a battery tester (Acutec Systems, Taiwan) at a current density of 5 mA cm^{-2} and a capacity of 1 mA h cm^{-2} over 2000 cycles. To ensure clarity, the acquired data were first processed with Microsoft Excel Visual Basic Application to pick out the maximum and minimum polarization potentials of each cycle, and then plotted. In the nucleation overpotential tests, a configuration similar to that of Li|Li symmetrical tests was employed. To rule out the over-potential caused by the diffusion of stripped Li ions through the GO coating, only the plating side was coated with GO. The coin cells were charged at a current density of 5 mA cm^{-2} for 100 s. Electronic impedance spectroscopy (EIS) of the symmetrical cells was performed from 0.1 MHz to 0.1 Hz with an amplitude of 10 mV, using a Solartron 1260 apparatus (Solartron, U.K.), and later fitted with Zview software (Scribner, USA). Cyclic voltammetry (CV) of GO was conducted with GO coated on the Cu working electrode and Li foil as the auxiliary and reference electrodes, using an electro-chemical workstation (Autolab PGSTAT302N, Netherlands). The scan rate was 0.1 mV s^{-1}, and the voltage window was from +3.3 to −0.15 V. Li−S cells were assembled with a round EG:S cathode having a diameter of 13 mm and a round Li foil having a diameter of 14 mm and a thickness of 300 μm on each side of the separator. To mitigate the shuttle effect,[32] one side of separator facing the cathode was spray-coated with GO from a solution of GO in acetone at a concentration of 2 g L^{-1}. The electrolyte was 1 M LiTFSI and 0.3 M $LiNO_3$ in DOL/DME (1:1, v/v). CV of the Li−S cells was conducted at a scan rate of 0.05 mV s^{-1} with a voltage window of 2.8 to 1.5 V. The galvanostatic charge/discharge performance of the Li−S cells was measured using a battery tester (Acutec Systems, Taiwan) over a voltage window of 2.8 to 1.5 V. The cells were activated by
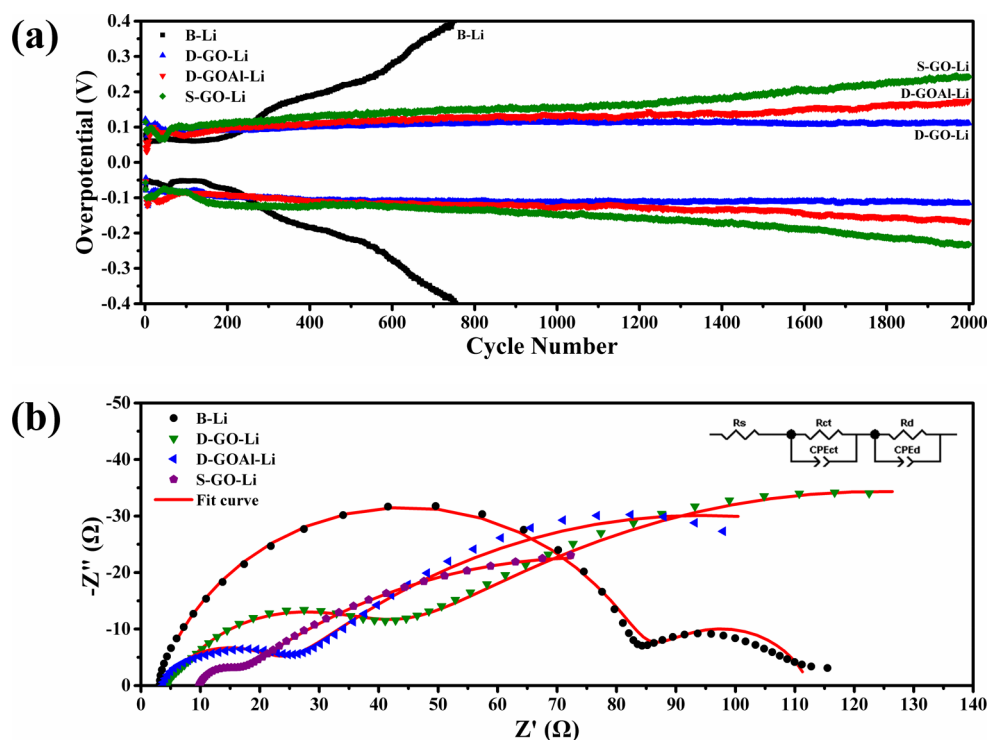
Figure 1. (a) Overpotential plotted with respect to cycle number for B-Li, D-GO-Li, D-GOAl-Li, and S-GO-Li symmetrical cells tested at a current density of 5 mA cm^{-2} and a deposition capacity of 1 mA h cm^{-2} for 2000 cycles. (b) The EIS and the circuit employed for fitting.

discharging at a constant current of 0.1 C (1 C = 1675 mA g^{-1}) to 1.5 V, followed by discharging at a constant voltage of 1.5 V to 0.01 C, and then charged at a constant current of 0.1 C to 2.8 V for three cycles. After activation, the cells were tested at 1 C with only constant current cycling.

Characterization. The morphologies of the GO materials were observed by first coating on top of Cu foil, following the same procedure for preparing D-GO-Li, and then examining with an FEI Nova 200 scanning electron microscope. To observe Li dendrites, the symmetrical cells after 2000 cycles were disassembled in an Ar-filled glove box. The Li anode was retreated, washed with DOL/DME (1:1, v/v), and dried for 24 h; then, it was transferred with a gas-sealed holder from the glove box to a Zeiss LEO-1530 scanning electron microscope. To measure the BET specific surface area and pore size distribution (Micromeritics ASAP 2020, USA), dry GO, GO-Al$_2$O$_3$, and Al$_2$O$_3$ nanoparticle powders were degassed at 250 °C for 24 h and followed by N$_2$ adsorption–desorption at 77 K. The reduction of GO during Li plating process was observed through X-ray photoelectron spectroscopy (XPS; PHI 5000 Versa Probe) equipped with an Al Kα X-ray source (1486.6 eV). Coin cells were assembled having a configuration identical to that for the GO CV study. Linear scan voltammetry (LSV) was applied to the cells from the open-circuit potential to 0 V at a scan rate of 0.1 mV s^{-1}, using an electrochemical workstation (Autolab PGSTAT302N, Netherlands). The cells before and after LSV were disassembled in an Ar-filled glove box. The working electrodes were retreated and washed with DOL/DME (1:1, v/v) solvent, dried for 24 h, and transferred into the XPS system. The acquired data were processed using CasaXPS software. C 1s XPS spectra were collected without etching and deconvoluted into graphitic, hydroxyl, carbonyl, and carboxylate signals.[33,34] Li 1s XPS spectra were collected after etching the surface of the GO with a 2 kV Ar ion beam for 5 min.

Assembly of Transparent Cells. In situ Li dendrite formation was observed in an air-tight glass bottle assembled in an Ar-filled glove box. Two pieces of Li foil of fixed dimensions were placed inside the bottle. The electrolyte was identical to that used in the symmetrical cells. The back side of each piece was covered with Kapton tape; the volume of the electrolyte was measured to ensure a fixed deposition

area. For the D-GO-Li sample, the coated sides of the two electrodes were facing each other. A current density of 5 mA cm^{-2} was applied to the cells for 30 min, and then the surface morphology of Li foil was recorded using an optical camera.

Simulation. Ab initio calculations for structural minimization and single-point energy calculations for the GO–GO and GO–Al$_2$O$_3$ systems were performed using a Vienna Ab-initio Simulation Package (VASP),[35−37] which is a plane-wave pseudopotential package based on the density functional theory (DFT). Generalized gradient approximation (GGA) was used, where the exchange-correlation functional between electrons was modeled using the Perdew−Burke−Ernzerhof (PBE) scheme,[38,39] and the projector augmented wave (PAW) method[40,41] was used for pseudopotentials. The kinetic energy cutoff for the plane-wave basis set of wave functions was 400 eV. The convergences of the self-consistent field were 10^{-6} eV for the energy and 10^{-3} eV Å^{-1} for the force. In describing the van der Waals (vdW) interactions in the modeling system, DFT-D3 with Becke−Johnson damping[42,43] was introduced as a semiempirical dispersion correction for the energy. GO was built at a C/O atomic ratio of 4:1, according to the XPS data in Figure S2 (Supporting Information). The binding energy E_b between GO and GO or between GO and Al$_2$O$_3$ was defined using the equation

$$E_b = E_{system} - (E_{GO} + E_{GO\ or\ Al_2O_3}) \tag{1}$$

where every term can be derived from individual single-point energy calculations using the minimized structures.

RESULTS AND DISCUSSION

To evaluate the dendrite suppression capability, Li|Li symmetrical cells were examined at a current density of 5 mA cm^{-2} and with a plating/stripping capacity of 1 mA h cm^{-2}. Figure 1a plots their overpotentials with respect to the cycle number, and the overpotential profiles from the selected cycles are shown in Figure S3 (Supporting Information). Below 200 cycles, B-Li exhibited the lowest overpotential of 60 mV; it was significantly lower than those of the other samples because, in
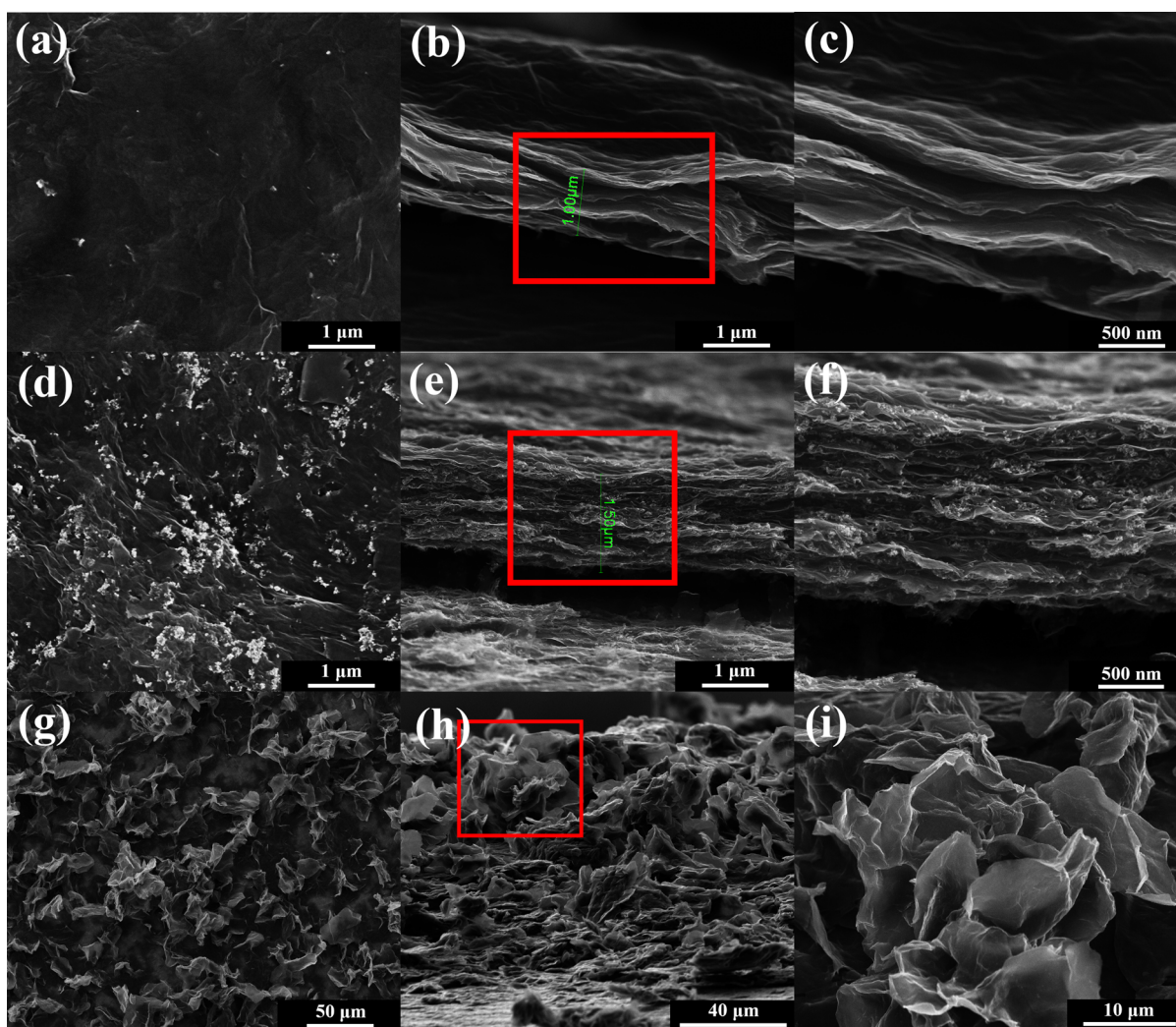
Figure 2. (a,d,g) Top-view and (b,c,e,f,h,i) cross-sectional SEM images of the GO layers of (a−c) D-GO-Li, (d−f) D-GOAl-Li, and (g−i) S-GO-Li.

the absence of a coating layer, the Li ions were not impeded from diffusing from the surface of the Li foil. This observation was consistent with the EIS of the symmetrical cells measured prior to cycling, presented in Figure 1b. The first semicircle, in the frequency range of approximately 0.1 MHz to 50 Hz, corresponded to charge transfer; the second corresponded to diffusion.[44,45] Table S1 (Supporting Information) lists the fitted values. Despite the charge transfer resistance of B-Li being greater than those of the other samples, the substantially lower diffusion resistance, resulting from the absence of GO layers through which the stripped Li ions had to diffuse, reversed the situation. Nevertheless, the overpotential escalated rapidly after 200 cycles and exceeded those of all the other samples after 300 cycles. The cell malfunctioned before 1000 cycles. Figure S4a−c (Supporting Information) presents the optical and scanning electron microscopy (SEM) images of B-Li after cycling. A thick layer of dead Li, resulting from the incipient inhomogeneity of both the solid electrolyte interphase (SEI) and the Li deposits,[46] covered the surface in the form of loosely packed needle-like dendrites of large surface area; these dendrites promoted the side reaction with the electrolyte and further formed large amounts of the SEI.[8] The accumulation of the SEI and dead Li would increase the resistance of the cell over time. Moreover, as displayed in Figure S5a (Supporting Information), the electric field tended

to concentrate at the tips of the dendrites to further aggravate the dendrite problem.[15,21] In contrast, the coated samples (Figure S4d−l, Supporting Information) all exhibited an instant increase in polarization (to ca. 100 mV) but stabilized within 150 cycles to finish the 2000 cycles without severely augmented polarization. During the deposition process, Li would first adhere to the surface of lithiophilic GO layers and some might migrate across the GO layers and deposit on Li metal surface.[21] Optical and SEM images (Figure S3d−l, Supporting Information) of the coated samples all revealed plated Li on top of the coating layer in a dense morphology without much protuberance, even in the most loosely packed areas (Figure S3f,i,l, Supporting Information). As a result, the dendrite formation was ameliorated, thanks to an evenly distributed electric field (Figure S5b, Supporting Information),[15,21] and the stability was improved in the coated samples, relative to B-Li.

Top-view and cross-sectional SEM images were recorded (Figure 2) to discriminate the morphological differences among the GO layers fabricated using the different coating procedures. The coating of D-GO-Li had the most well-aligned compact layered structure and the smoothest surface. The thickness of the layer was approximately 1 μm. The coating of D-GOAl-Li had a mesoporous structure and a thickness of 1.5 μm. Compared with that of D-GO-Li, the D-GOAl-Li surface

was full of wrinkles, and Al$_2$O$_3$ nanoparticles appeared as white spots. The coating of S-GO-Li had a macroporous structure, with a crumpled GO layer piled up randomly. This structure covered the surface of the Li foil inefficiently; as such, a thickness of 100 μm (substantially greater than the coatings of D-GO-Li and D-GOAl-Li) was required to form a uniform black coating. Because of the light weight and low thickness of the GO coatings, the energy density of the modified anodes was unaffected. Scheme 1 illustrates the coating procedures

Scheme 1. In D-GO-Li the Compact GO Coating Will Hamper Li Stripping during the First Activation Discharging Process in Li−S Cells, while in D-GOAl-Li the Loosely Packed GO-Al$_2$O$_3$ Composite Coating Will Alleviate Such Adversity. In S-GO-Li, an Extremely Loosely Packed GO Can Be Obtained Using the Spray-Coating Method, and Li Ions Can Pass through the Coating Layer Even Easier.
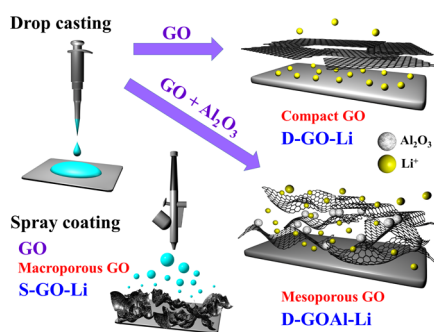
and the self-assembly mechanism. During the drop-casting procedure, it took a relatively long time for the THF to evaporate. Prior to completion of its evaporation, the layers of pure GO remained flexible and unconfined. These layers could stretch and stack in such a manner that the interactions between them were the strongest. This mechanism resulted in a compact and smooth morphology. Figure S6 (Supporting Information) presents the results of simulations of the GO−GO and GO−Al$_2$O$_3$ interactions. When the whole structure reached the required convergence, binding energies for GO−GO and GO−Al$_2$O$_3$ were −1.797 and −3.959 eV, respectively. Because of the latter's greater binding energy, the Al$_2$O$_3$ nanoparticles attached themselves to the GO layers and anchored the layers firmly together, thereby inhibiting the layers from stretching into smooth surfaces. As a result, severely wrinkled GO layers piled up to form a mesoporous structure. The ability of Al$_2$O$_3$ nanoparticles to create a mesoporous structure was further proved by BET specific area and pore size distribution, as shown in Figure S7 (Supporting Information). GO−Al$_2$O$_3$ exhibited a larger surface area (105 m^2 g^{-1}) than GO (8.31 m^2 g^{-1}). The mesoporous GO−Al$_2$O$_3$ exhibited a type IV absorption−desorption isotherm, with a peak situated at 10 to 100 nm in the pore size distribution graph, in agreement with the SEM image. During the spray-coating procedure, the GO solution was transferred to the Li foil in the form of fine droplets; the huge total surface area of the droplets shortened the evaporation time of the THF. Shrinkage of the droplets crumpled the GO layers prior to their reaching the surface. As a result, the crumpled GO layers piled up to form a macroporous structure.
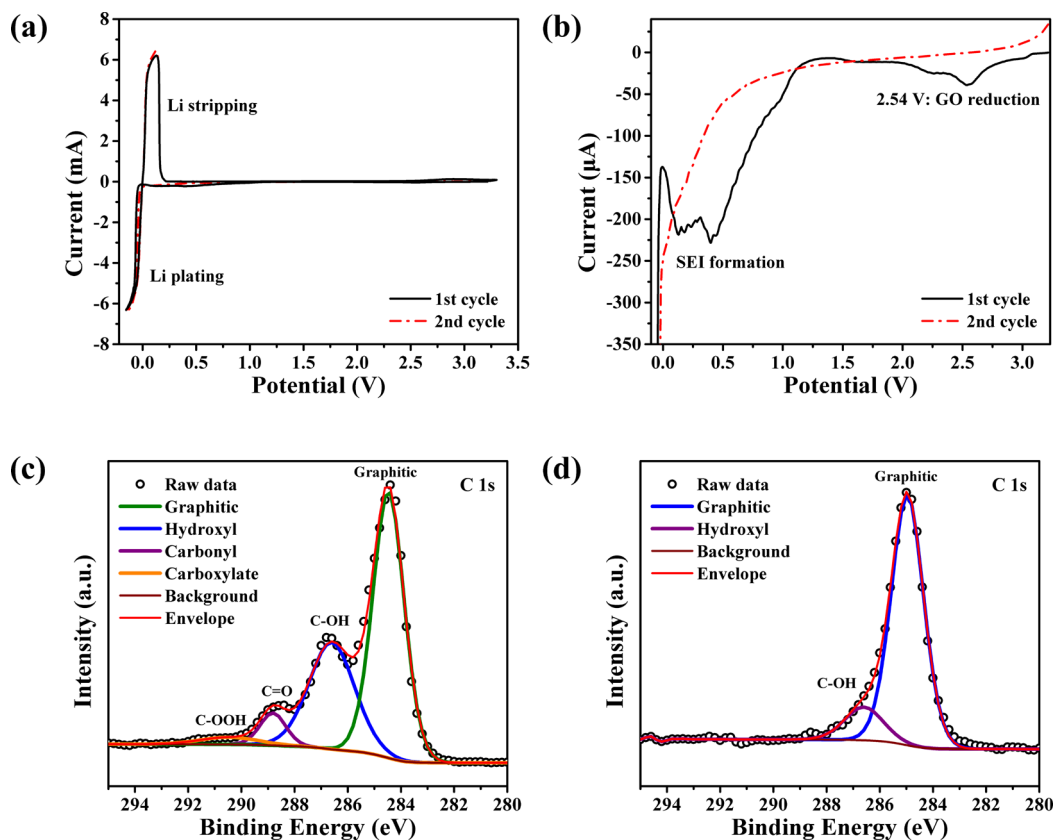

Figure 3. (a) Full-view and (b) expanded cathodic portion of the CV trace of GO. C 1s XPS spectra of GO (c) before and (d) after LSV.
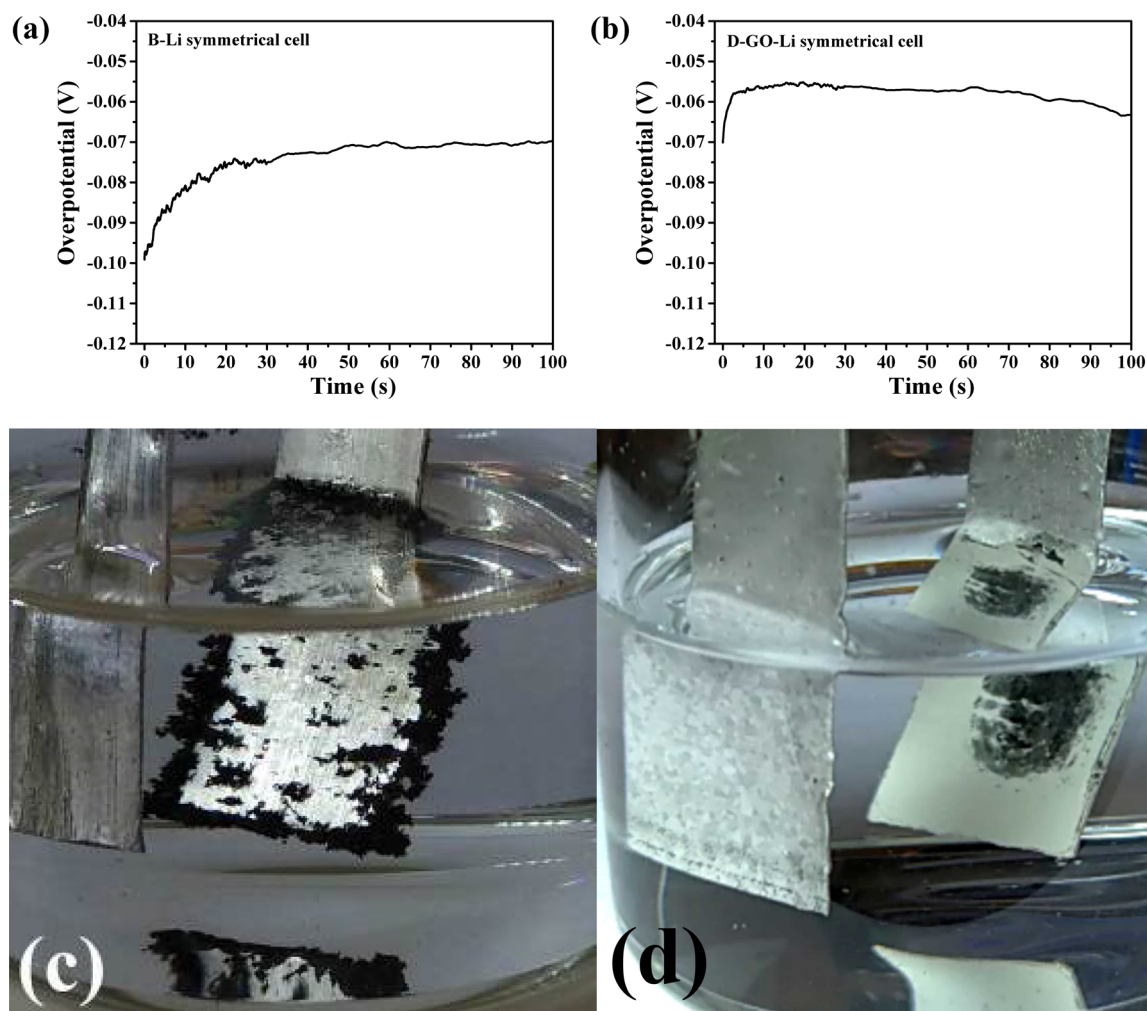
Figure 4. Nucleation overpotentials of (a) B-Li and (b) D-GO-Li. Transparent cells of (c) B-Li and (d) D-GO-Li.

The morphological differences among the samples played crucial roles affecting the cell performance and stability. As displayed in Figure 1a, after being subjected to 2000 cycles, D-GO-Li exhibited the lowest degree of polarization, whereas S-GO-Li had the highest. The coating having a macroporous morphology featured a greater surface area and more open spaces for attack from the electrolyte, and therefore, similar to carbon electrode materials,[47] it was more susceptible to SEI formation. The mesoporous structure possessed a moderate surface area and less open space than the macroporous structure, whereas the compact structure had the least. Excessive SEI would lead to increased resistance and, thus, increased polarization. As a consequence, D-GO-Li, which had a compact structure, exhibited the highest stability; S-GO-Li was the worst, and D-GOAl-Li was in between the two. The EIS performance, however, followed the opposite trend. Figure 1b reveals that S-GO-Li exhibited both the lowest charge transfer and the lowest diffusion resistance, whereas D-GO-Li exhibited the worst. Prior to the formation of the SEI, the larger surface area and more open environment resulting from the macroporous morphology facilitated the Li deposition reaction. In the macroporous structure, the stripped Li ions could also diffuse through a less tortuous path, which was beneficial for lowering the diffusion resistance,[48] because there were more wider tunnels. With its larger reaction area and faster diffusion kinetics, S-GO-Li appears potentially suitable

for applications requiring high power density.[47] In the compact structure, a less effective surface area for the charge transfer reaction and a more tortuous diffusion path resulted in larger impedance. The mesoporous structure displayed performance between those of the macroporous and compact structures. Nevertheless, the addition of the Al_2O_3 nanoparticles led to questionable performance from D-GOAl-Li, because the ability to suppress dendrites might have arisen solely from the presence of Al_2O_3. Hence, symmetrical cells featuring Li foil coated with only Al_2O_3 nanoparticles were prepared to prove that the dendrite suppression ability of D-GOAl-Li was contributed primarily by the synergistic effect between GO and the Al_2O_3 nanoparticles. Figure S9 (Supporting Information) presents the corresponding polarization chart and Nyquist plot. The polarization of the sample containing the Al_2O_3 nanoparticles, being analogues to B-Li, increased rapidly prior to 1000 cycles being reached and even exhibited both greater charge transfer and greater diffusion impedance than B-Li. Hence, the Al_2O_3 nanoparticles were ineffective at suppressing dendrite formation.

To understand the mechanism behind dendrite suppression, the Sand's time model should be considered. Despite the fact that it was originally proposed to describe the evolution of H_2 during Cu plating in a solution of H_2SO_4 and $CuSO_4$,[49] the Sand's time model has been modified and adapted to describe the formation of Li dendrites and has revealed that decreasing
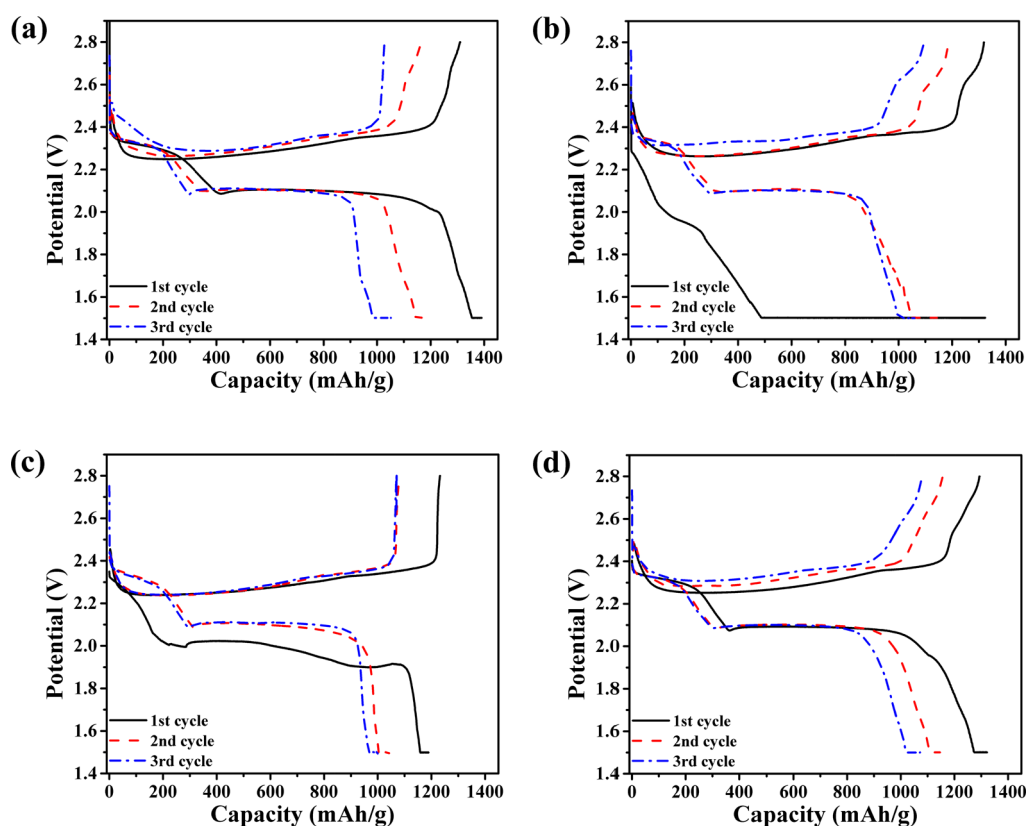
Figure 5. Three activation cycles of (a) B-Li, (b) D-GO-Li, (c) D-GOAl-Li, and (d) S-GO-Li incorporated within Li−S cells.

the current density would be effective in suppressing dendrite formation.[50,51] On the other hand, because of the strong reducing nature of Li metal, virtually any electrolyte would form an SEI on contact with Li metal,[52] and the local current density would increase if any inhomogeneity or defect existed on the SEI layer. The GO layers presumably possessed electrochemical properties that could alleviate such problems. CV was conducted to observe the electrochemical behavior of the GO layers during the incipient charging stage (Figure 3a,b). The open-circuit potential of the as-assembled cell was 3.3 V, and large Li stripping and plating peaks appeared near 0 V. When the current scale was widened, a GO reduction peak appeared with an onset potential of 2.7 V versus Li/Li$^+$ in DME/DOL (1:1, v/v); this onset potential is analogous to reported values of −0.5 and −0.7 V versus H$_2$/H$^+$ in aqueous solution.[34,53] Peaks also appeared before 0 V, attributable to the SEI formation.[5,20] Figure 3c,d present the C 1s XPS spectra of GO before and after performing LSV. The acquired signal was deconvoluted into signals for graphitic, hydroxyl, carbonyl, and carboxylic carbon atoms.[33,34] After LSV, the intensities of the C 1s peaks of higher binding energy decreased/disappeared and the sample was reduced to a lower oxidation state, in agreement with the CV data. This finding indicated that the GO layer would automatically undergo reduction during operation of the cells. The reduced GO layers transformed into conductive scaffolds[29] and could decrease both the local current density and electric field by distributing the current density more evenly.[54] A longer Sand's time was, therefore, acquired—and it resulted in a lower tendency for dendrite formation.[50]

In addition to confirming the enhanced conductivity of the reduced GO, the lithiophilicity of the GO layers was evaluated

by observing the nucleation overpotential. During the galvanostatic Li plating process, the overpotential can be separated into two components: the nucleation overpotential and the plateau overpotential.[12] Upon charging, the over-potential decreased immediately because of the extra energy required for incubation of the Li nuclei; later, it resurged toward the asymptotical value, which was the plateau overpotential required for steady current flow. In Figure 4a,b, the asymptotical values for B-Li and D-GO-Li are −0.07 and −0.06 V, respectively. The minor difference might have arisen from slight inconsistencies during the cell assembly. After subtracting the plateau overpotential from the onset potential, nucleation overpotentials for B-Li and D-GO-Li were 0.03 and 0.01 V, respectively. The result confirmed that the lithiophilicity of GO was greater than that of the SEI on the surface of the Li metal. Lithium tends to wet a substrate with greater lithiophilicity and, thus, increase the reaction surface, leading to a decrease in local current density and a prolonged Sand's time. These phenomena could be visualized after the fabrication of transparent cells. In Figure 4c,d, a localized Li deposition is evident in B-Li; it would result in a higher local current density and, thus, more severe dendrite formation.[11] In contrast, Li was plated more evenly in the D-GO-Li sample, owing to the higher lithiophilicity of GO.[17] An evenly distributed morphology would decrease the local current density and alleviate dendrite formation.[5] The complete plating process for B-Li and D-GO-Li is presented in Movies S1 and S2 (Supporting Information), respectively. The Li metal was attached more evenly and closer to the GO coating, while it kept breaking loose from the bare Li surface, confirming the effectiveness of the GO layers in suppressing Li dendrites.
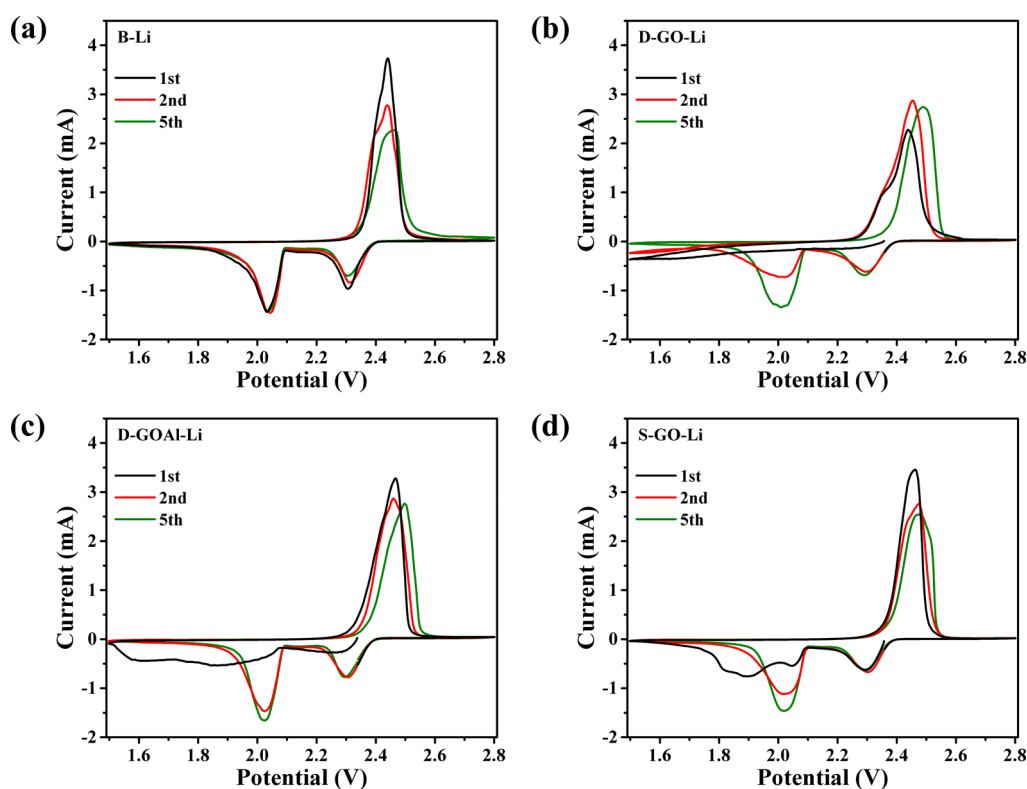
G

Figure 6. CV traces of (a) B-Li, (b) D-GO-Li, (c) D-GOAl-Li, and (d) S-GO-Li incorporated within Li−S cells.

The Li 1s XPS spectra were recorded before and after performing LSV to investigate whether Li ions could be transported or deposited inside the GO layers. Figure S10 (Supporting Information) reveals that Li could be detected after LSV, confirming the ability of the GO layers to transport or accommodate Li. The enhancement in conductivity after reduction, the high lithiophilicity, and the capability to transport Li ions all rendered GO as a good material for the suppression of dendrite formation.

To test the applicability of the GO coatings, the modified Li anodes were incorporated with sulfur cathodes and a GO-coated separator was employed to mitigate the shuttle effect.[32] Figure S11 (Supporting Information) presents top-view and cross-sectional images of the GO-coated separator. The separator was fully covered by a smooth GO film having a thickness of 0.8 μm. Figure 5 presents the three activation cycles of the galvanostatic charge/discharge test of the Li−S cells incorporating B-Li, D-GO-Li, D-GOAl-Li, and S-GO-Li. All these cells could achieve a capacity of approximately 1200 mA h g⁻¹. B-Li provided the smoothest discharge curve with the least polarization, implying the fastest reaction kinetics among these samples.[55] Two sharp plateaus appeared, corresponding to the reduction of sulfur (S_8) to long-chain polysulfides (Li_2S_x; $x = 4−8$; $E = 2.3$ V) and the reduction of long-chain polysulfides to Li_2S_2 or Li_2S ($E = 2.1$ V).[56,57] The curves for all the coated samples exhibited greater polarization in the first activation cycle, compared with that of B-Li, because all the stripped Li ions had to diffuse through the coating layers. The first discharge curve with barely discernable plateaus for D-GO-Li decreased rapidly and severely tailed during the constant-voltage discharging step, indicative of sluggish kinetics during the Li stripping process, due to the compact GO layer. When featuring a mesoporous coating, a curve with a more evident, but distorted, plateau appeared,

indicative of improved Li stripping kinetics when compared with that of D-GO-Li. S-GO-Li provided a discharge profile similar to B-Li, except for slightly duller turning at the end of the second plateau; it possessed the best kinetic properties among all the coated samples. This result is positively related to the diffusion resistance acquired in the EIS measurements in Figure 1b. During the first cycle, Li ion flow would create defects on GO layers and facilitate the diffusion process.[21] Moreover, part of the Li would deposit on top of the GO coatings when charging, reducing Li ions required for stripping from under the GO coating, thereby resulting in significantly better reaction kinetics in the following discharge process. Hence, the shapes of the second and third discharge curves of all the coated samples became more similar to that for B-Li.

Figure 6 presents CV traces of the Li−S batteries. B-Li provided two cathodic peaks, corresponding to the reduction of sulfur to long-chain polysulfides and the reduction of long-chain polysulfides to Li_2S_2 or Li_2S, with onset potentials of 2.4 and 2.1 V, respectively.[56,57] The anodic peak referring to the oxidation of Li sulfides had an onset potential of 2.3 V. During the first cycle, the cathodic peaks for all the coated samples featured a low height and a trailing tail. The peak height for D-GO-Li was the lowest, whereas that for S-GO-Li was the highest. The Randles−Sevcik equation is[58]

$$i_p = 0.4463nFAC\left(\frac{nF\nu D}{RT}\right)^{1/2}$$

(2)

where n is the number of electrons transferred in the redox event, A is the electrode area in cm², F is the Faraday current, C is the concentration in mol cm⁻³, ν is the scan rate in V s⁻¹, R is the gas constant, and T is the temperature in K. A lower diffusion coefficient would lead to a lower peak current. This behavior indicated the generally worse diffusion kinetics in the

H

coated samples and increasing diffusion kinetics upon proceeding from D-GO-Li through D-GOAl-Li to S-GO-Li. The increasing height of the cathodic peaks during the second cycle, for all the samples, implied improved Li stripping kinetics. The CV data were in good agreement with the galvanostatic charge/discharge tests, as well as the EIS results.

The long-term cyclability of the Li−S cells under 1 C (1675 mA h g^{-1}) is presented in Figure 7, and the charge-discharge
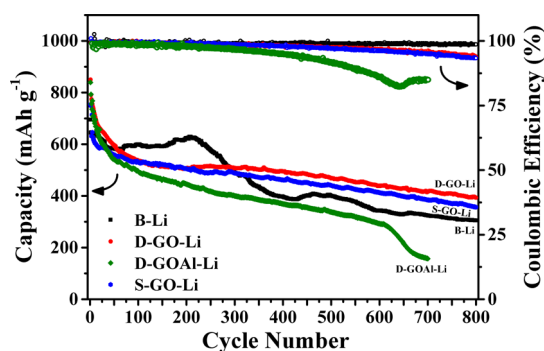

Figure 7. Capacity retention and coulombic efficiency, plotted with respect to the cycle number, for B-Li, D-GO-Li, D-GOAl-Li, and S-GO-Li incorporated within Li−S cells cycled at a C-rate of 1 C.

curves from the selected cycles are shown in Figure S12. B-Li exhibited the best capacity of 600 mA h g^{-1} within 200 cycles, but it degraded dramatically, to less than 400 mA h g^{-1}, after 400 cycles. Although D-GO-Li displayed a lower capacity than B-Li initially, it maintained capacities of 500 mA h g^{-1} after 400 cycles and 400 mA h g^{-1} after 800 cycles. S-GO-Li also preserved a good capacity over 800 cycles, but it was 50 mA h g^{-1} lower than that of D-GO-Li because of the slightly poorer stability of the macroporous structure relative to the compact structure. Neither of the samples experienced a sudden drop in capacity near 200 cycles, owing to the Li suppression ability of the GO coatings. Unfortunately, D-GOAl-Li exhibited poor capacity after the onset of the test, because of the polysulfide absorption ability of Al$_2$O$_3$,[59] which increased the probability of side reactions between the polysulfides and Li and resulted in the loss of the cathode material and an insidious compound forming on top of the anode. Nevertheless, the concept of fabricating this GO-Al$_2$O$_3$ composite could be extended by replacing Al$_2$O$_3$ with other materials having lower affinity toward polysulfides and greater lithiophilicity, thereby potentially improving the performance.

CONCLUSIONS

GO layers have been coated on top of Li metal anodes through drop-casting and spray-coating. With these different coating procedures and the synergistic effect of Al$_2$O$_3$ nanoparticles, the GO self-assembled into three different morphologies: compact, mesoporous, and macroporous structures. In symmetrical cell tests performed at a current density of 5 mA cm^{-2} and a capacity of 1 mA h cm^{-2}, all the coated samples could complete 2000 cycles without any short circuiting or any dramatic increases in polarization. During cell operation, the GO coating transformed into reduced GO with higher conductivity and, thus, decreased the local current density by distributing the current more evenly. A longer Sand's time and a greater lithiophilicity rendered GO as a good coating material for suppressing the formation of Li dendrites. This study

provides insight into how the morphologies of coatings can influence cell performance: macroporous coatings with lower degrees of charge-transfer and diffusion impedance are suitable for applications requiring high power density, whereas compact coatings with outstanding stability are more suitable for long-life products. The GO coatings were incorporated into Li−S cells that exhibited improved capacity retention after 800 cycles, compared with that of the bare Li anode, suggesting potential applications for such materials in new-generation Li-ion batteries.

ASSOCIATED CONTENT

$\ominus$ Supporting Information

The Supporting Information is available free of charge on the ACS Publications website at DOI: 10.1021/acsami.8b18379.

> Overpotentials plotted with respect to the cycle number for D-GO-Li symmetrical cells featuring various GO loadings and sample coated with Al$_2$O$_3$ nanoparticles; XPS Li 1s and full spectrum of GO; overpotential plots for symmetrical cells from selected cycles; fitted values of EIS; optical and SEM images of Li metal anodes after symmetrical cell tests; schematic representations of Li metal anodes with and without GO coatings; interactions within GO−GO and GO−Al$_2$O$_3$ structures; BET measurement for GO, GO−Al$_2$O$_3$, and Al$_2$O$_3$ nanoparticles; SEM of GO-coated separator; charge−discharge curve for Li−S cells from selected cycles (PDF)

> Complete Li plating process of B-Li (MPG)

> Complete Li plating process of D-GO-Li (MPG)

AUTHOR INFORMATION

Corresponding Author

*E-mail: gchu@gate.sinica.edu.tw.

ORCID 🄳

Yu-Ting Chen: 0000-0001-9525-8407

Karunakara Moorthy Boopathi: 0000-0003-2042-9595

Chun-Wei Pao: 0000-0003-0821-7856

Chih-Wei Chu: 0000-0003-0979-1729

Notes

The authors declare no competing financial interest.

ACKNOWLEDGMENTS

REFERENCES

(1) Cheng, X.-B.; Zhang, Q. Dendrite-Free Lithium Metal Anodes: Stable Solid Electrolyte Interphases for High-Efficiency Batteries. *J. Mater. Chem. A* **2015**, *3*, 7207−7209.

(2) Sun, Y.; Liu, N.; Cui, Y. Promises and Challenges of Nanomaterials for Lithium-Based Rechargeable Batteries. *Nat. Energy* **2016**, *1*, 16071.

(3) Xu, W.; Wang, J.; Ding, F.; Chen, X.; Nasybulin, E.; Zhang, Y.; Zhang, J.-G. Lithium Metal Anodes for Rechargeable Batteries. *Energy Environ. Sci.* **2014**, *7*, 513−537.

(4) Jin, S.; Sun, Z.; Guo, Y.; Qi, Z.; Guo, C.; Kong, X.; Zhu, Y.; Ji, H. High Areal Capacity and Lithium Utilization in Anodes Made of Covalently Connected Graphite Microtubes. *Adv. Mater.* **2017**, *29*, 1700783.

(5) Zhang, R.; Cheng, X. B.; Zhao, C. Z.; Peng, H. J.; Shi, J. L.; Huang, J. Q.; Wang, J.; Wei, F.; Zhang, Q. Conductive Nanostructured Scaffolds Render Low Local Current Density to Inhibit Lithium Dendrite Growth. *Adv. Mater.* **2016**, *28*, 2155−2162.

(6) Albertus, P.; Babinec, S.; Litzelman, S.; Newman, A. Status and Challenges in Enabling the Lithium Metal Electrode for High-Energy and Low-Cost Rechargeable Batteries. *Nat. Energy* **2018**, *3*, 16−21.

(7) Armand, M.; Tarascon, J.-M. Issues and Challenges Facing Rechargeable Lithium Batteries. *Nature* **2001**, *414*, 359−367.

(8) Cheng, X.-B.; Zhang, R.; Zhao, C.-Z.; Zhang, Q. Toward Safe Lithium Metal Anode in Rechargeable Batteries: A Review. *Chem. Rev.* **2017**, *117*, 10403−10473.

(9) Ling, C.; Banerjee, D.; Matsui, M. Study of The Electrochemical Deposition of Mg in The Atomic Level: Why It Prefers the Non-Dendritic Morphology. *Electrochim. Acta* **2012**, *76*, 270−274.

(10) Jäckle, M.; Groß, A. Microscopic Properties of Lithium, Sodium, and Magnesium Battery Anode Materials Related to Possible Dendrite Growth. *J. Chem. Phys.* **2014**, *141*, 174710.

(11) Nishikawa, K.; Mori, T.; Nishida, T.; Fukunaka, Y.; Rosso, M. Li Dendrite Growth and Li+ Ionic Mass Transfer Phenomenon. *J. Electroanal. Chem.* **2011**, *661*, 84−89.

(12) Pei, A.; Zheng, G.; Shi, F.; Li, Y.; Cui, Y. Nanoscale Nucleation and Growth of Electrodeposited Lithium Metal. *Nano Lett.* **2017**, *17*, 1132−1139.

(13) Yan, K.; Lu, Z.; Lee, H.-W.; Xiong, F.; Hsu, P.-C.; Li, Y.; Zhao, J.; Chu, S.; Cui, Y. Selective Deposition and Stable Encapsulation of Lithium Through Heterogeneous Seeded Growth. *Nat. Energy* **2016**, *1*, 16010.

(14) Park, K.; Goodenough, J. B. Dendrite-Suppressed Lithium Plating from a Liquid Electrolyte via Wetting of Li_3N. *Adv. Energy Mater.* **2017**, *7*, 1700732.

(15) Cheng, X. B.; Hou, T. Z.; Zhang, R.; Peng, H. J.; Zhao, C. Z.; Huang, J. Q.; Zhang, Q. Dendrite-Free Lithium Deposition Induced by Uniformly Distributed Lithium Ions for Efficient Lithium Metal Batteries. *Adv. Mater.* **2016**, *28*, 2888−2895.

(16) Ding, F.; Xu, W.; Chen, X.; Zhang, J.; Shao, Y.; Engelhard, M. H.; Zhang, Y.; Blake, T. A.; Graff, G. L.; Liu, X.; Zhang, J.-G. Effects of Cesium Cations in Lithium Deposition via Self-Healing Electrostatic Shield Mechanism. *J. Phys. Chem. C* **2014**, *118*, 4043−4049.

(17) Lin, D.; Liu, Y.; Liang, Z.; Lee, H. W.; Sun, J.; Wang, H.; Yan, K.; Xie, J.; Cui, Y. Layered Reduced Graphene Oxide with Nanoscale Interlayer Gaps as a Stable Host for Lithium Metal Anodes. *Nat. Nanotechnol.* **2016**, *11*, 626−632.

(18) Tsai, C. L.; Roddatis, V.; Chandran, C. V.; Ma, Q.; Uhlenbruck, S.; Bram, M.; Heitjans, P.; Guillon, O. $Li_7La_3Zr_2O_{12}$ Interface Modification for Li Dendrite Prevention. *ACS Appl. Mater. Interfaces* **2016**, *8*, 10617−10626.

(19) Chen, Y.-T.; Jena, A.; Pang, W. K.; Peterson, V. K.; Sheu, H.-S.; Chang, H.; Liu, R.-S. Voltammetric Enhancement of Li-Ion Conduction in Al-Doped $Li_{7−x}La_3Zr_2O_{12}$ Solid Electrolyte. *J. Phys. Chem. C* **2017**, *121*, 15565−15573.

(20) Xie, K.; Yuan, K.; Zhang, K.; Shen, C.; Lv, W.; Liu, X.; Wang, J. G.; Wei, B. Dual Functionalities of Carbon Nanotube Films for Dendrite-Free and High Energy-High Power Lithium-Sulfur Batteries. *ACS Appl. Mater. Interfaces* **2017**, *9*, 4605−4613.

(21) Foroozan, T.; Soto, F. A.; Yurkiv, V.; Sharifi-Asl, S.; Deivanayagam, R.; Huang, Z.; Rojaee, R.; Mashayek, F.; Balbuena, P. B.; Shahbazian-Yassar, R. Synergistic Effect of Graphene Oxide for Impeding the Dendritic Plating of Li. *Adv. Funct. Mater.* **2018**, *28*, 1705917.

(22) Bai, M.; Xie, K.; Yuan, K.; Zhang, K.; Li, N.; Shen, C.; Lai, Y.; Vajtai, R.; Ajayan, P.; Wei, B. A Scalable Approach to Dendrite-Free Lithium Anodes via Spontaneous Reduction of Spray-Coated Graphene Oxide Layers. *Adv. Mater.* **2018**, *30*, 1801213.

(23) Bobnar, J.; Lozinsek, M.; Kapun, G.; Njel, C.; Dedryvere, R.; Genorio, B.; Dominko, R. Fluorinated Reduced Graphene Oxide as a Protective Layer on the Metallic Lithium for Application in the High Energy Batteries. *Sci. Rep.* **2018**, *8*, 5819.

(24) Manthiram, A.; Fu, Y.; Chung, S.-H.; Zu, C.; Su, Y.-S. Rechargeable Lithium−Sulfur Batteries. *Chem. Rev.* **2014**, *114*, 11751−11787.

(25) Xu, G.; Ding, B.; Pan, J.; Nie, P.; Shen, L.; Zhang, X. High Performance Lithium−Sulfur Batteries: Advances and Challenges. *J. Mater. Chem. A* **2014**, *2*, 12662−12676.

(26) Yang, Y.; Zheng, G.; Cui, Y. Nanostructured Sulfur Cathodes. *Chem. Soc. Rev.* **2013**, *42*, 3018−3032.

(27) Manthiram, A.; Fu, Y.; Su, Y.-S. Challenges and Prospects of Lithium−Sulfur Batteries. *Acc. Chem. Res.* **2013**, *46*, 1125−1134.

(28) Bruce, P. G.; Freunberger, S. A.; Hardwick, L. J.; Tarascon, J. M. Li-O_2 and Li-S Batteries with High Energy Storage. *Nat. Mater.* **2011**, *11*, 19−29.

(29) Mohan, V. B.; Brown, R.; Jayaraman, K.; Bhattacharyya, D. Characterisation of Reduced Graphene Oxide: Effects of Reduction Variables on Electrical Conductivity. *Mater. Sci. Eng., B* **2015**, *193*, 49−60.

(30) Paredes, J. I.; Villar-Rodil, S.; Martínez-Alonso, A.; Tascon, J. M. D. Graphene Oxide Dispersions in Organic Solvents. *Langmuir* **2008**, *24*, 10560−10564.

(31) Konios, D.; Stylianakis, M. M.; Stratakis, E.; Kymakis, E. Dispersion Behaviour of Graphene Oxide and Reduced Graphene Oxide. *J. Colloid Interface Sci.* **2014**, *430*, 108−112.

(32) Jiang, Y.; Chen, F.; Gao, Y.; Wang, Y.; Wang, S.; Gao, Q.; Jiao, Z.; Zhao, B.; Chen, Z. Inhibiting the Shuttle Effect of Li−S Battery with a Graphene Oxide Coating Separator: Performance Improvement and Mechanism Study. *J. Power Sources* **2017**, *342*, 929−938.

(33) Oh, J.-S.; Hwang, T.; Nam, G.-Y.; Hong, J.-P.; Bae, A.-H.; Son, S.-I.; Lee, G.-H.; Sung, H. K.; Choi, H. R.; Koo, J. C.; Nam, J.-D. Chemically-Modified Graphene Sheets as an Active Layer for Eco-Friendly Metal Electroplating on Plastic Substrates. *Thin Solid Films* **2012**, *521*, 270−274.

(34) Zhou, M.; Wang, Y.; Zhai, Y.; Zhai, J.; Ren, W.; Wang, F.; Dong, S. Controlled Synthesis of Large-Area and Patterned Electrochemically Reduced Graphene Oxide Films. *Chem. - Eur. J.* **2009**, *15*, 6116−6120.

(35) Kresse, G.; Hafner, J. Ab Initio Molecular Dynamics for Liquid Metals. *Phys. Rev. B* **1993**, *47*, 558−561.

(36) Kresse, G.; Hafner, J. Ab Initio Molecular Dynamics for Open-Shell Transition Metals. *Phys. Rev. B* **1993**, *48*, 13115−13118.

(37) Kresse, G.; Hafner, J. Ab Initio Molecular-Dynamics Simulation of The Liquid-Metal−Amorphous-Semiconductor Transition in Germanium. *Phys. Rev. B* **1994**, *49*, 14251−14269.

(38) Perdew, J. P.; Chevary, J. A.; Vosko, S. H.; Jackson, K. A.; Pederson, M. R.; Singh, D. J.; Fiolhais, C. Atoms, Molecules, Solids, and Surfaces: Applications of the Generalized Gradient Approximation for Exchange and Correlation. *Phys. Rev. B* **1992**, *46*, 6671−6687.

(39) Perdew, J. P.; Wang, Y. Accurate and Simple Analytic Representation of the Electron-Gas Correlation Energy. *Phys. Rev. B* **1992**, *45*, 13244−13249.

(40) Blöchl, P. E. Projector Augmented-Wave Method. *Phys. Rev. B* **1994**, *50*, 17953−17979.

(41) Kresse, G.; Joubert, D. From Ultrasoft Pseudopotentials to the Projector Augmented-Wave Method. *Phys. Rev. B* **1999**, *59*, 1758−1775.

(42) Grimme, S.; Antony, J.; Ehrlich, S.; Krieg, H. A Consistent and Accurate Ab Initio Parametrization of Density Functional Dispersion Correction (DFT-D) for the 94 Elements H-Pu. *J. Chem. Phys.* **2010**, *132*, 154104.

(43) Grimme, S.; Ehrlich, S.; Goerigk, L. Effect of the Damping Function in Dispersion Corrected Density Functional Theory. *J. Comput. Chem.* **2011**, *32*, 1456−1465.

(44) Aksakal, C.; Sisman, A. On the Compatibility of Electric Equivalent Circuit Models for Enhanced Flooded Lead Acid Batteries Based on Electrochemical Impedance Spectroscopy. *Energies* **2018**, *11*, 118.

(45) Landesfeind, J.; Pritzl, D.; Gasteiger, H. A. An Analysis Protocol for Three-Electrode Li-Ion Battery Impedance Spectra: Part I.

Analysis of a High-Voltage Positive Electrode. *J. Electrochem. Soc.* **2017**, *164*, A1773−A1783.

(46) Stark, J. K.; Ding, Y.; Kohl, P. A. Nucleation of Electro-deposited Lithium Metal: Dendritic Growth and the Effect of Co-Deposited Sodium. *J. Electrochem. Soc.* **2013**, *160*, D337−D342.

(47) An, S. J.; Li, J.; Daniel, C.; Mohanty, D.; Nagpure, S.; Wood, D. L. The State of Understanding of the Lithium-Ion-Battery Graphite Solid Electrolyte Interphase (SEI) and Its Relationship to Formation Cycling. *Carbon* **2016**, *105*, 52−76.

(48) Cooper, S. J.; Bertei, A.; Finegan, D. P.; Brandon, N. P. Simulated Impedance of Diffusion in Porous Media. *Electrochim. Acta* **2017**, *251*, 681−689.

(49) Sand, H. J. S. III. On the Concentration at the Electrodes in a Solution, with Special Reference to the Liberation of Hydrogen by Electrolysis of a Mixture of Copper Sulphate and Sulphuric Acid. *Lond. Edinb. Dubl. Phil. Mag.* **1901**, *1*, 45−79.

(50) Brissot, C.; Rosso, M.; Chazalviel, J.-N.; Lascaud, S. Dendritic Growth Mechanisms in Lithium/Polymer Cells. *J. Power Sources* **1999**, *81−82*, 925−929.

(51) Rosso, M.; Brissot, C.; Teyssot, A.; Dollé, M.; Sannier, L.; Tarascon, J.-M.; Bouchet, R.; Lascaud, S. Dendrite Short-Circuit and Fuse Effect on Li/Polymer/Li cells. *Electrochim. Acta* **2006**, *51*, 5334−5340.

(52) Lin, D.; Liu, Y.; Cui, Y. Reviving the Lithium Metal Anode for High-Energy Batteries. *Nat. Nanotechnol.* **2017**, *12*, 194−206.

(53) Shao, Y.; Wang, J.; Engelhard, M.; Wang, C.; Lin, Y. Facile and Controllable Electrochemical Reduction of Graphene Oxide and Its Applications. *J. Mater. Chem.* **2010**, *20*, 743−748.

(54) Cheng, X. B.; Peng, H. J.; Huang, J. Q.; Wei, F.; Zhang, Q. Dendrite-Free Nanostructured Anode: Entrapment of Lithium in a 3D Fibrous Matrix for Ultra-Stable Lithium-Sulfur Batteries. *Small* **2014**, *10*, 4257−4263.

(55) Fan, F. Y.; Chiang, Y.-M. Electrodeposition Kinetics in Li-S Batteries: Effects of Low Electrolyte/Sulfur Ratios and Deposition Surface Composition. *J. Electrochem. Soc.* **2017**, *164*, A917−A922.

(56) Abbas, S. A.; Ding, J.; Wu, S. H.; Fang, J.; Boopathi, K. M.; Mohapatra, A.; Lee, L. W.; Wang, P. C.; Chang, C. C.; Chu, C. W. Modified Separator Performing Dual Physical/Chemical Roles to Inhibit Polysulfide Shuttle Resulting in Ultrastable Li-S Batteries. *ACS Nano* **2017**, *11*, 12436−12445.

(57) Abbas, S. A.; Ibrahem, M. A.; Hu, L.-H.; Lin, C.-N.; Fang, J.; Boopathi, K. M.; Wang, P.-C.; Li, L.-J.; Chu, C.-W. Bifunctional Separator as a Polysulfide Mediator for Highly Stable Li−S Batteries. *J. Mater. Chem. A* **2016**, *4*, 9661−9669.

(58) Oldham, K. B. Analytical Expressions for the Reversible Randles−Sevcik Function. *J. Electroanal. Chem. Interfacial Electrochem.* **1979**, *105*, 373−375.

(59) Tao, X.; Wang, J.; Liu, C.; Wang, H.; Yao, H.; Zheng, G.; Seh, Z. W.; Cai, Q.; Li, W.; Zhou, G.; Zu, C.; Cui, Y. Balancing Surface Adsorption and Diffusion of Lithium-Polysulfides on Nonconductive Oxides for Lithium-Sulfur Battery Design. *Nat. Commun.* **2016**, *7*, 11203.